Physics – Uspekhi **55** (11) 1140 – 1151 (2012)

CONFERENCES AND SYMPOSIA

PACS numbers: 01.10.Fv, 65.80.Ck, 68.65.Pq, 72.15.Jf, 72.20.Pa, 72.80.Vp, 78.67.Wj, 81.05.ue

Physical properties of graphene
(Scientific session of the Physical Sciences Division of the Russian Academy of Sciences, 28 March 2012)

DOI: 10.3367/UFNe.0182.201211h.1223

A scientific session of the Physical Sciences Division of the Russian Academy of Sciences (RAS) devoted to the "Physical properties of graphene" was held on 28 March 2012 in the conference hall of the Lebedev Physical Institute.

The agenda of the session announced on the RAS Physical Sciences Division website www.gpad.ac.ru included the following reports:

(1) **Falkovsky L A** (Landau Institute of Theoretical Physics, RAS, Moscow; Vereshchagin Institute of High-Pressure Physics, RAS, Moscow) "Magnetooptics of graphene";

(2) **Varlamov A A** (The University of Rome Tor Vergata, Italy) "Thermoelectric properties of graphene."

The papers written on the basis of these reports are given below.

PACS numbers: 68.65.Pq, 78.67.Wj, 81.05.ue
DOI: 10.3367/UFNe.0182.201211i.1223

Magnetooptics of graphene layers

L A Falkovsky

1. Introduction

Most of the vast amount of information on graphene can be described based on the concept of "gapless Dirac fermions." According to this concept, at the K points of the Brillouin zone (vertices of a hexagon), there are two zones without a gap between them, and the electron spectrum can be considered linear in a sufficiently wide neighborhood of wave vectors. It is obvious that to assume the spectrum to be linear, the size of the neighborhood under consideration must be small compared to the size of the Brillouin zone, i.e., less than 10^8 cm^{-1}, which suggests not too large concentrations of charge carriers, $n \ll 10^{16}$ cm^{-2}. Ideally pure graphene at zero temperature should contain no charge carriers at all, and the Fermi level should separate the conduction band from the valence band. However, it is quite difficult to prepare pure graphene; the minimum concentration of charge carriers that could be obtained in it to date is $n \sim 10^9$ cm^{-2}. The following key problems arise here: to what extent the Coulomb electron interaction renormalizes the initial linear spectrum and whether graphene can pass into a state with an energy gap.

At present, there is also a practical need in gapped materials for modern electronics. Therefore, investigations of a graphene bilayer to which a constant voltage can be applied (as to a capacitor), thereby creating an energy gap in its spectrum, have become quite popular. In its development over the last half-century, physics has come full circle and returned to the investigation of graphite. Here, we recall the names of Slonczewski and Weiss [1], who formulated the principle of the description of a layered substance with a strong interaction in the layers and a weak interaction between them.

The main methods for studying the metallic state appear to be magnetotransport and magnetooptical investigations. In a magnetic field, phenomena such as Hall effects (classical and quantum) are observed, as is rotation of the polarization plane, or the Faraday effect upon light transmission and the Kerr effect upon reflection. In describing graphene layers, in spite of the relative simplicity of the presented picture, difficulties arise, which, just as the corresponding achievements, are the subject of this paper.

2. Electronic spectrum of graphene

The K points of the Brillouin zone have the C_{3v} symmetry (a 3-fold axis and a symmetry plane). This space group has a two-dimensional representation whose basis is composed of two functions that are transformed into one another under reflection and acquire factors $\exp(\pm 2\pi i/3)$ under rotation. Using the components of the momentum deviation from the K points, linear combinations $k_\pm = \mp i k_x - k_y$ can be composed that transform similarly to the functions of the basis. The effective Hamiltonian must be invariant under a representation of this small group; hence, near the K point, we have a unique possibility of writing the Hamiltonian in the linear approximation:

$$H(\mathbf{k}) = \begin{pmatrix} 0 & vk_+ \\ vk_- & 0 \end{pmatrix}, \qquad (1)$$

L A Falkovsky Landau Institute of Theoretical Physics, Russian Academy of Sciences, Moscow, Russian Federation; Vereshchagin Institute of High-Pressure Physics, Russian Academy of Sciences, Moscow, Russian Federation
E-mail: falk@itp.ac.ru

Uspekhi Fizicheskikh Nauk **182** (11) 1223 – 1234 (2012)
DOI: 10.3367/UFNr.0182.201211h.1223
Translated by S N Gorin; edited by A M Semikhatov

Uspekhi Fizicheskikh Nauk **182** (11) 1223 – 1229 (2012)
DOI: 10.3367/UFNr.0182.201211i.1223
Translated by S N Gorin; edited A M Semikhatov

where v is a constant with the dimension of velocity. The same Hamiltonian is obtained, naturally, in the tight-binding approximation.

The eigenvalues of the matrix in the right-hand side of Eqn (1) give a two-band gapless spectrum:

$$\varepsilon_{1,2} = \mp v\sqrt{k_x^2 + k_y^2} = \mp vk\,.$$

Hence, the gapless character of the spectrum is a mere consequence of the symmetry, and the fact that the Fermi level should pass through the conical point K follows merely from the valence of carbon. The cyclotron mass for such a spectrum is given by

$$m(\varepsilon) = \frac{1}{2\pi}\,\frac{\mathrm{d}S(\varepsilon)}{\mathrm{d}\varepsilon} = \frac{\varepsilon}{v^2}\,,$$

where S is the area of the cross section of the isoenergy surface and the concentration of charge carriers at zero temperature is expressed through the chemical potential μ as

$$n(\mu) = \frac{\mu^2}{\pi\hbar^2 v^2}\,.$$

The simplest way to experimentally verify the type of spectrum is by using the relation

$$m(\mu)\,\frac{v}{\hbar} = \mp\sqrt{\pi n(\mu)}\,,$$

for example, by measuring the Shubnikov–de Haas effect, in which case the cyclotron mass at the Fermi level is found from the temperature dependence of the amplitude of oscillations and the concentration of charge carriers is determined from their frequency. Both these quantities are measured at different concentrations of charge carriers, which is changed by varying the voltage at the ''gate.'' Such a verification was performed by Ellis et al. [2], who obtained very pure samples with a charge-carrier concentration as low as 10^9 cm^{-2}. It turned out that the ''constant'' parameter v is not constant but increases at small concentrations by a factor of three compared to its ''normal'' value 10^8 cm s^{-1} at concentrations exceeding 10^{11} cm^{-2}. This effect is a result of the electron–electron Coulomb interaction, which proves to be more efficient, as was to be expected, at small concentrations, when no screening is observed. The logarithmic renormalization of the velocity due to the Coulomb interaction in the three-dimensional case was first found in [3], and for two-dimensional graphene, in [4]. Interestingly, even at a quite low concentration, no signs of any phase transition have been found. In accordance with the theory, the Coulomb interaction does not violate the symmetry-related gapless character of the spectrum.

3. Dynamic conductivity of graphene

One of the clearest manifestations of the specific character of the graphene spectrum can be provided by the behavior of its dynamic (i.e., frequency-dependent) conductivity (conductance). At higher frequencies, in the optical range, the spatial dispersion of conductivity and the frequency of collisions of charge carriers are insignificant. Summing the contributions from conical points (two per unit cell), integrating over the angle of the two-dimensional vector $\mathbf{k}$, and passing to the variable $\varepsilon = vk$, we find the conductivity as [5–7]

$$\sigma(\omega) = \frac{e^2\omega}{\mathrm{i}\pi\hbar}\left[\int_{-\infty}^{+\infty}\mathrm{d}\varepsilon\,\frac{|\varepsilon|}{\omega^2}\,\frac{\mathrm{d}f(\varepsilon)}{\mathrm{d}\varepsilon} - \int_0^{+\infty}\mathrm{d}\varepsilon\,\frac{f(-\varepsilon)-f(\varepsilon)}{(\omega+\mathrm{i}\delta)^2-4\varepsilon^2}\right], \tag{2}$$

where $f(\varepsilon)$ is the distribution function and δ is an infinitesimal parameter. The first term in the right-hand side of Eqn (2), which represents the intraband contribution, can be integrated once more:

$$\sigma^{\mathrm{intra}}(\omega) = \frac{2\mathrm{i}e^2T}{\pi\hbar(\omega+\mathrm{i}\tau^{-1})}\ln\left(2\cosh\frac{\mu}{2T}\right), \tag{3}$$

where we substituted $\omega + \mathrm{i}\tau^{-1}$ for ω in order to allow for the electron relaxation τ. In this form, the intraband contribution coincides with the classical Drude–Boltzmann expression for conductivity. At low temperatures ($\mu \gg T$), when the charge carriers are degenerate, the intraband term acquires a ''metallic'' form:

$$\sigma^{\mathrm{intra}}(\omega) = \frac{\mathrm{i}e^2|\mu|}{\pi\hbar(\omega+\mathrm{i}\tau^{-1})}\,. \tag{4}$$

For pure graphene, the chemical potential is $\mu = 0$ (gapless dielectric) and conductivity (3) is proportional to the temperature. The concentration of charge carriers can be changed either by doping or by applying a constant electric field (''field effect'').

The second term in the right-hand side of Eqn (2), where δ is an infinitesimal quantity describing interband transitions, contains both a real part, which arises as a result of going around the pole and corresponds to absorption, and an imaginary part. At zero temperature, the second integral in the right-hand side of Eqn (2) can be calculated analytically as

$$\sigma^{\mathrm{inter}}(\omega) = \frac{e^2}{4\hbar}\left[\theta(\omega-2\mu) - \frac{\mathrm{i}}{2\pi}\ln\frac{(\omega+2\mu)^2}{(\omega-2\mu)^2}\right], \tag{5}$$

where θ is the step-function, which reflects the condition of interband electron transitions with the threshold $\omega = 2\mu$. The logarithmic singularity is removed by a temperature cut-off (or by relaxation of charge carriers), and at a finite but small (in comparison with the chemical potential) temperature, the following replacement should be made in (5):

$$\begin{aligned}&\theta(\omega-2\mu) \to \frac{1}{2} + \frac{1}{\pi}\arctan\left(\frac{\omega-2\mu}{2T}\right),\\ &(\omega-2\mu)^2 \to (\omega-2\mu)^2 + (2T)^2\,.\end{aligned} \tag{6}$$

The above results allow arriving at two main conclusions. First, at high frequencies $\omega \gg (T, \mu)$, the conductivity is mainly real and independent of any parameters:

$$\sigma(\omega) = \frac{e^2}{4\hbar}\,.$$

In this frequency range, which is limited from above by the band width (of about 3 eV), the conductivity, as we see, is independent of the material parameters, e.g., of the velocity v, and has a universal character. Second, if degenerate carriers exist in graphene at sufficiently low temperatures, then the imaginary part of the conductivity contains a logarithmic singularity at the threshold of the interband absorption $\omega = 2\mu$, where the real part undergoes a finite jump. This feature becomes smoothened with increasing the temperature

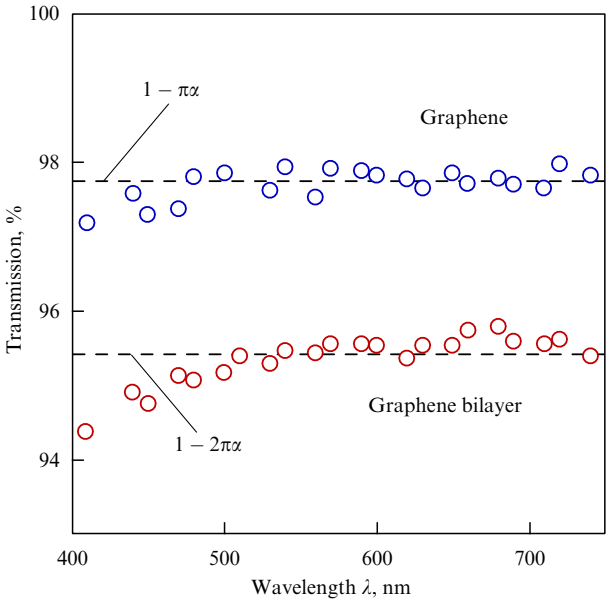

Figure 1. The coefficient of light transmission through graphene and a graphene bilayer [11].

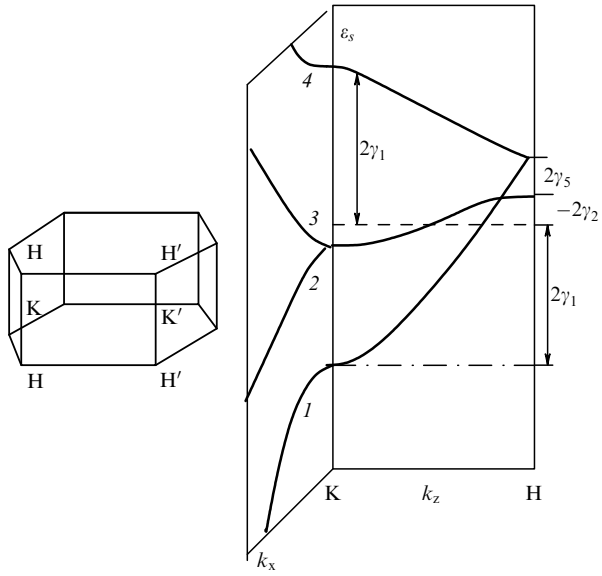

Figure 2. The Brillouin zone and the electron spectrum of graphite.

and also because of the finite length of the mean free path of charge carriers. To observe this feature, the frequency should not exceed the temperature, i.e., should be of the order of 10–40 K in energy units. These conclusions have been confirmed experimentally [8].

The universal conductivity leads to an interesting consequence. Using its value, the coefficient of transmission T of an electromagnetic wave through graphene can be obtained as [9, 10]

$$T = 1 - \frac{4\pi}{c}\,\mathrm{Re}\,\sigma(\omega)\cos\theta = 1 - \pi\,\frac{e^2}{\hbar c}\cos\theta\,, \qquad (7)$$

where θ is the incidence angle of the wave. We see that the coefficient of light transmission through a graphene layer is expressed via the fine-structure constant of quantum electrodynamics, to which graphene has no relation at all. Several experimental groups [11, 12] have confirmed the calculated value of the transmission coefficient in a wide frequency range of the visible spectrum, both for graphene and for a graphene bilayer, in which the difference of this coefficient from unity is twice greater (Fig. 1).

4. Spectrum of graphene layers in a magnetic field

The Slonczewski–Weiss Hamiltonian for a graphene bilayer and graphite in the vicinity of the KH line of the Brillouin zone has the form

$$H(\mathbf{k}) = \begin{pmatrix} \tilde\gamma_5 + U & vk_+ & \tilde\gamma_1 & \dfrac{\tilde\gamma_4 vk_-}{\gamma_0} \\ vk_- & \tilde\gamma_2 + U & \dfrac{\tilde\gamma_4 vk_-}{\gamma_0} & \dfrac{\tilde\gamma_3 vk_+}{\gamma_0} \\ \tilde\gamma_1 & \dfrac{\tilde\gamma_4 vk_+}{\gamma_0} & \tilde\gamma_5 - U & vk_- \\ \dfrac{\tilde\gamma_4 vk_+}{\gamma_0} & \dfrac{\tilde\gamma_3 vk_-}{\gamma_0} & vk_+ & \tilde\gamma_2 - U \end{pmatrix}, \qquad (8)$$

where $k_\pm = \mp \mathrm{i}k_x - k_y$ is the projection of the quasimomentum, v is the parameter of the velocity in the direction of graphite layers, $\tilde\gamma_j$ are functions of the projection k_z in the direction of the principal axis,

$$\tilde\gamma_2 = 2\gamma_2\cos(2k_z d_0)\,, \quad \tilde\gamma_5 = 2\gamma_5\cos(2k_z d_0) + \Delta\,,$$

$$\tilde\gamma_i = 2\gamma_i\cos(k_z d_0)\,, \quad i = 1, 3, 4,$$

and $d_0 = 3.35$ Å is the spacing between the layers in graphite.

The velocity parameter $v = 1.5a_0\gamma_0 = 10^8$ cm s^{-1} is related to the overlap ($\gamma_0 \approx 3$ eV) of the wave functions of nearest neighbors located in the same layer at the distance $a_0 = 1.415$ Å from each other. The parameters with $i = 1, 3, 4$, which arise because of the overlap of the wave functions of nearest neighbors in the direction of the principal axis, are an order of magnitude less than γ_0. In a bilayer, there is only one neighboring layer in the direction of the principal axis; therefore, $\tilde\gamma_i = \gamma_i$ for $i = 1, 3, 4$, and because the next layer is absent, the interlayer integrals of the overlap with the third sphere are $\tilde\gamma_i = 0$ for $i = 2, 5$, whereas they should be taken into account in graphite.

In the absence of a magnetic field, the spectrum can be computed numerically (Fig. 2) and studied analytically [13]; the specific features of conductivity related to transitions between the bands can also be studied experimentally. Hamiltonian (8) also involves the parameter U, which is important in the case of a bilayer when a constant voltage is applied to it in the direction of the principal axis. At an arbitrary value of the quasimomentum, we find four energy eigenvalues, which are numbered using subscripts $s = 1, 2, 3, 4$. At $k_x = k_y = 0$ (i.e., on the KH line) and $U = 0$, there is a twofold degeneracy ($\varepsilon_2 = \varepsilon_3$), which is a consequence of the symmetry. In an external electric field U, a gap appears in the spectrum; it is this feature that mainly accounts for the enhanced interest in bilayers. In addition, the simple quadratic behavior in the bands that touch each other acquires the shape of a Mexican hat. There is one more detail that should be taken into account: two points, K and K′, which pass into one another under rotations and

reflection ($x \to -x$), are not equivalent in the bilayer; the reflection corresponds to the permutation $k_+ \leftrightarrow k_-$ in Hamiltonian (1). To avoid the enumeration of obvious possibilities, we restrict ourselves to the description of the graphite spectrum at $U = 0$ and only then turn to a bilayer.

The problem becomes more complex and more interesting in the presence of a magnetic field. In a magnetic field B that is parallel to the principal axis, the projections of the quasi-momentum $k_{x,y}$ are operators with the commutation relation $\{\hat{k}_+, \hat{k}_-\} = -2e\hbar B/c$; it is therefore convenient to introduce creation and annihilation operators a^+ and a that change the Landau index by unity:

$$\hat{k}_+ = \sqrt{\frac{2|e|\hbar B}{c}}\, a\,, \quad \hat{k}_- = \sqrt{\frac{2|e|\hbar B}{c}}\, a^+\,.$$

For graphene, an explicit expression for the spectrum is found using Eqn (1) in the form

$$\varepsilon_{1,2} = \mp v\sqrt{\frac{2|e|\hbar B n}{c}}\,,$$

where $n = 0, 1, \ldots$.

The eigensolutions for matrix Hamiltonian (8) are sought in the form of a column,

$$\psi^{\alpha}_{sn}(x) = \begin{Bmatrix} C^1_{sn}\varphi_{n-1}(x) \\ C^2_{sn}\varphi_n(x) \\ C^3_{sn}\varphi_{n-1}(x) \\ C^4_{sn}\varphi_{n-2}(x) \end{Bmatrix}, \tag{9}$$

where $\varphi_n(x)$ are the orthogonal Hermite functions with the Landau eigenvalue $n \geqslant 0$. At a given n, the states are numbered by the band index $s = 1, 2, 3, 4$; we use the notation $|sn\rangle$ for states by counting s, as before, from below. For brevity, we omit the standard exponentials that appear in the Landau gauge and take the degeneracy in corresponding components of the quasimomentum into account only in the final results.

It is easy to see that if we neglect terms with γ_3, which lead to a trigonal warping of the spectrum, then each line of matrix Hamiltonian (8) is proportional to a certain Hermite function, which can therefore be canceled. We thus come to the problem for eigenvectors $\mathbf{C}_{sn}$ and eigenvalues

$$\begin{pmatrix} \tilde{\gamma}_5 - \varepsilon & \omega_c\sqrt{n} & \tilde{\gamma}_1 & \omega_4\sqrt{n-1} \\ \omega_c\sqrt{n} & \tilde{\gamma}_2 - \varepsilon & \omega_4\sqrt{n} & 0 \\ \tilde{\gamma}_1 & \omega_4\sqrt{n} & \tilde{\gamma}_5 - \varepsilon & \omega_c\sqrt{n-1} \\ \omega_4\sqrt{n-1} & 0 & \omega_c\sqrt{n-1} & \tilde{\gamma}_2 - \varepsilon \end{pmatrix} \begin{Bmatrix} C^1_{sn} \\ C^2_{sn} \\ C^3_{sn} \\ C^4_{sn} \end{Bmatrix} = 0\,, \tag{10}$$

where $\omega_c = v\sqrt{2|e|\hbar B/c}$, $\omega_4 = \tilde{\gamma}_4\omega_c/\gamma_0$.

We see from (9) that at $n = 0$, the eigenvector has one nonzero component, $\mathbf{C}_0 = (0, 1, 0, 0)$, and there is only one (rather than four) energy eigenvalue

$$\varepsilon(n = 0) = \tilde{\gamma}_2\,, \tag{11}$$

which depends on k_z and intersects the Fermi level such that electrons appear in the vicinity of the K point (up to the Fermi level) and holes appear in the vicinity of the H point (Fig. 3).

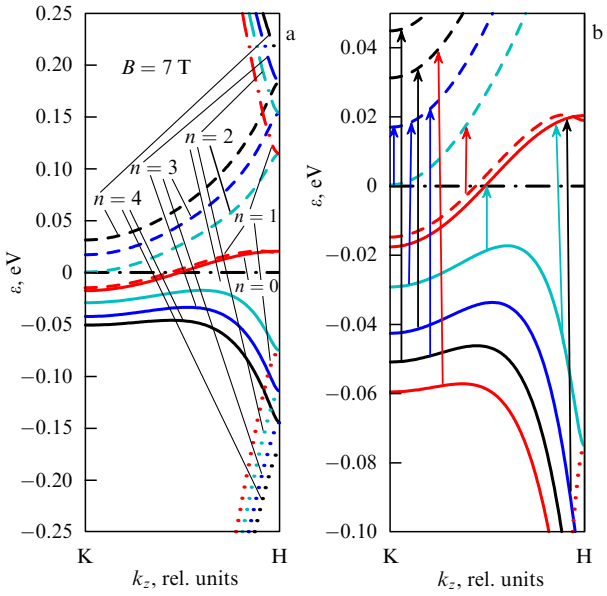

Figure 3. (Available in color online.) (a) Landau levels ε_{sn} from $n = 0$ to $n = 4$ in four bands, $s = 1, 2, 3, 4$ (dotted, solid, dashed, and dotted-and-dashed curves, respectively), depending on the projection of the momentum k_z along the KH line in the Brillouin zone of graphite ($K = 0$, $\mathrm{H} = \pi/2d_0$) for a magnetic field $B = 7$ T; the band parameters are given in the table. (b) An enlarged fragment of Fig. 3a for the bands $s = 2$ and 3.

At $n = 1$, we see from Eqns (9) that the fourth component should be set equal to zero ($C^4_{s1} = 0$), and three (rather than four) levels can be determined from the first three equations. The middle level $|21\rangle$ is very close to $|10\rangle$, and in the region of k_z where the condition $\gamma_1/\cos z \gg \gamma_2$ holds and where the electrons are located, this level has the energy

$$\varepsilon_2(n = 1) = \tilde{\gamma}_2 - 2\,\frac{\omega_c^2\,\tilde{\gamma}_4}{\tilde{\gamma}_1\gamma_0}\,. \tag{12}$$

For $n \geqslant 2$, four eigenvalues exist at any k_z. The energies of two close levels with $s = 2$ and 3 in the region $\gamma_1/\cos z \gg \gamma_2$, where electrons are located, are expressed as

$$\varepsilon_{2,3}(n) = \tilde{\gamma}_2 - \frac{\omega_c^2\,\tilde{\gamma}_4}{\tilde{\gamma}_1\gamma_0}\,(2n-1) \mp \frac{\omega_c^2}{\tilde{\gamma}_1}\,\sqrt{n(n-1)}\,. \tag{13}$$

4.1 Effect of a trigonal distortion on the spectrum in a magnetic field

In spite of the smallness of the ratio γ_3/γ_0, the effect of trigonal distortion is significant because of the degeneracy that is observed in the KH lines. To date, several ways to take the trigonal distortion into account have been suggested. Two of these are analytic: the perturbation theory [14] and semiclassical quantization [15]. The perturbation theory for the matrix Hamiltonian can suitably be constructed based on its Green's function

$$G_0^{\alpha\beta}(\varepsilon, x, x') = \sum_{sn} \frac{\psi^{\alpha}_{sn}(x)\,\psi^{*\beta}_{sn}(x')}{\varepsilon - \varepsilon_{sn}}\,, \tag{14}$$

where the superscripts can take four values, in accordance with the matrix of the Hamiltonian, and x and x' are position variables.

In the second approximation, we obtain the correction

$$\int \mathrm{d}x_1\,\mathrm{d}x_2\,G_0^{\alpha 4}(x,x_1)\,V^{42}(x_1)\,G_0^{22}(x_1,x_2)\,V^{24}(x_2)\,G_0^{4\beta}(x_2,x')\,,$$

and a similar term with the permutation of indices $2 \leftrightarrow 4$. The matrix elements of the perturbation V, labeled by the superscripts, can be easily calculated using functions (9); for the correction to the Green's function (14), we obtain the expression

$$\left(\frac{\omega_c\tilde{\gamma}_3}{\gamma_0}\right)^2 \sum_{s'sn} \frac{(n-2)|C_{sn}^4 C_{s',n-3}^2|^2 \psi_{sn}^{\alpha}(x)\,\psi_{sn}^{*\beta}(x')}{(\varepsilon-\varepsilon_{sn})(\varepsilon-\varepsilon_{s',n-3})(\varepsilon-\varepsilon_{sn})}\,. \qquad (15)$$

Correction (15) is large near the poles of the Green's function. Therefore, for ε close to ε_{sn}, we can substitute ε_{sn} in the second factor in the denominator instead of ε. Thus, the Green's function with the correction is written as

$$\frac{1}{\varepsilon-\varepsilon_{sn}} + \frac{\delta}{(\varepsilon-\varepsilon_{sn})^2}\,,$$

which, up to terms of the second order in δ, can be represented as

$$\frac{1}{\varepsilon-\varepsilon_{sn}-\delta}\,.$$

The expression obtained from (15) allows writing a correction to the eigenvalue in the form

$$\delta\varepsilon_s(n) = \left(\frac{\omega_c\tilde{\gamma}_3}{\gamma_0}\right)^2 \sum_{s'} \left[\frac{(n-2)|C_{sn}^4 C_{s',n-3}^2|^2}{\varepsilon_s(n)-\varepsilon_{s'}(n-3)} + \frac{(n+1)|C_{sn}^2 C_{s',n+3}^4|^2}{\varepsilon_s(n)-\varepsilon_{s'}(n+3)}\right], \qquad (16)$$

where the terms with $n-3<0$ can be omitted.

Formula (16) contains a parameter of the perturbation theory. We note that the spacing between the unperturbed levels can be estimated, for example, using Eqn (13). We thus find this dimensionless parameter

$$\left(\frac{\tilde{\gamma}_3\tilde{\gamma}_1}{\gamma_0\omega_c}\right)^2,$$

which turns out to be less than unity in magnetic fields $B \gg 1$ T. We also write the level $|10\rangle$ with the correction:

$$\varepsilon_1(n=0) = \tilde{\gamma}_2 + \left(\frac{\omega_c\tilde{\gamma}_3}{\gamma_0}\right)^2 \sum_{s'} \frac{|C_{s'3}^4|^2}{\tilde{\gamma}_2-\varepsilon_{s'}(3)}\,. \qquad (17)$$

The band structure in a magnetic field is shown in Fig. 3. A comparison shows that our expressions (16) and (17) for the levels give the same results as the numerical method of truncating an infinite-rank matrix [16]. We note that the expressions obtained are also applicable to a bilayer; we only should set $\gamma_2=\gamma_5=0$ and $\tilde{\gamma}_i=\gamma_i$ for $i=1, 3, 4$ and take the field U into account.

The semiclassical quantization, which we do not describe here, can suitably be introduced in the case of weak magnetic fields and relatively pure materials with a small frequency of collisions, when the observation of quantum oscillations is still possible.

5. Transmission coefficient and the magnetooptical effect in graphene layers

In the presence of a magnetic field, a radically new phenomenon is the appearance of the Hall component of conductivity, which is usually denoted by $\sigma_{xy}(\omega)$. The Hall conductivity violates the rotation symmetry about the principal axis, which leads to Faraday and Kerr effects, i.e., to the rotation of the polarization plane of light during its transmission and reflection. Electron transitions then become possible, both between band states s and between different Landau levels n; therefore, resonance denominators $\Delta_{ss'n}=\varepsilon_{sn}-\varepsilon_{s',n+1}$ appear. The method for calculating the correlator that determines the current and is expressed through the product of two Green's functions remains essentially the same as in the absence of a magnetic field.

The calculations in [13] lead to the following expressions for the two components of conductivity of graphite in the collisionless case, where the frequency of collisions Γ is much less than the spacing between the levels:

$$\left\{\begin{matrix}\sigma_{xx}(\omega)\\ \mathrm{i}\sigma_{xy}(\omega)\end{matrix}\right\} = \mathrm{i}\sigma_0\,\frac{4\omega_c^2}{\pi^2}\sum_{n,s,s'}\int_0^{\pi/2}\mathrm{d}z\,\frac{\Delta f_{ss'n}}{\Delta_{ss'n}}\,|\mathrm{d}_{ss'n}|^2 \times\left[(\omega+\mathrm{i}\Gamma+\Delta_{ss'n})^{-1}\pm(\omega+\mathrm{i}\Gamma-\Delta_{ss'n})^{-1}\right], \qquad (18)$$

where the integration is performed over one-half of the Brillouin zone, $0<z<\pi/2$; in the case of graphene and a bilayer, it is not performed. Here, $\Delta f_{ss'n}=f(\varepsilon_{s'n+1})-f(\varepsilon_{sn})$ is the difference of distribution functions with the shift of levels due to trigonal distortion taken into account, and the matrix element of the dipole moment

$$d_{ss'n}=C_{sn}^2C_{s'n+1}^1+C_{sn}^3C_{s'n+1}^4+\frac{\tilde{\gamma}_4}{\gamma_0}\,(C_{sn}^1C_{s'n+1}^4+C_{sn}^2C_{s'n+1}^3)$$

is expressed in terms of the components of wave function (9). The most intense electron transitions that are taken into account satisfy the selection rule $\Delta n=1$.

In addition, the renormalization of the dipole moment, in other words, of the electron–photon vertex, due to the trigonal distortion must be taken into account. This renormalization leads to additional weak lines, obtained by replacing the matrix element in (18) by the quantity

$$d_{ss'n}=\frac{\tilde{\gamma}_3}{\gamma_0}\,C_{sn}^2C_{s'n+2}^4$$

and by the replacement $n+1\to n+2$ with the new selection rule $\Delta n=2$.

The results of calculations are shown in Figs 4 and 5. The Kerr rotation angle reaches giant values, which exceed the values typical of semiconductors by more than an order of magnitude. The oscillations of the angle are related to certain electron transitions, and the position of its maxima (as well as of reflection minima) are determined either by the boundaries of the Landau levels at the K and H points or by the intersection of these levels with the Fermi level (Fig. 3b). We note that the dispersion of the levels affects the positions of optical features. We used the parameters of Hamiltonian (8) presented in the table. Their values (also see [19, 20]) differ from those obtained in various experimental studies only because we took a different form of the Hamiltonian than the one used by Slonczewski and Weiss (the third line of the

Table. Parameters of Hamiltonian (8), their relation to the Slonczewski–Weiss (SW) notation, and the numerical values (in meV) obtained in experimental work [17, 18].

Hamiltonian (8)	γ_0	γ_1	γ_2	γ_3	γ_4	γ_5	Δ	ε_F
	3050	360	−10.2	270	−150	−1.5	16	−4.1
SW [1]	γ_0	γ_1	$2\gamma_2$	γ_3	$-\gamma_4$	$2\gamma_5$	$\Delta + 2(\gamma_2 - \gamma_5)$	$2\gamma_2 + \varepsilon_F$
Mendez et al. [17]	3160	390	− 20	276	44	38	8	−24
Doezema et al. [18]	3120	380	−21	315	120	−3	−2	—

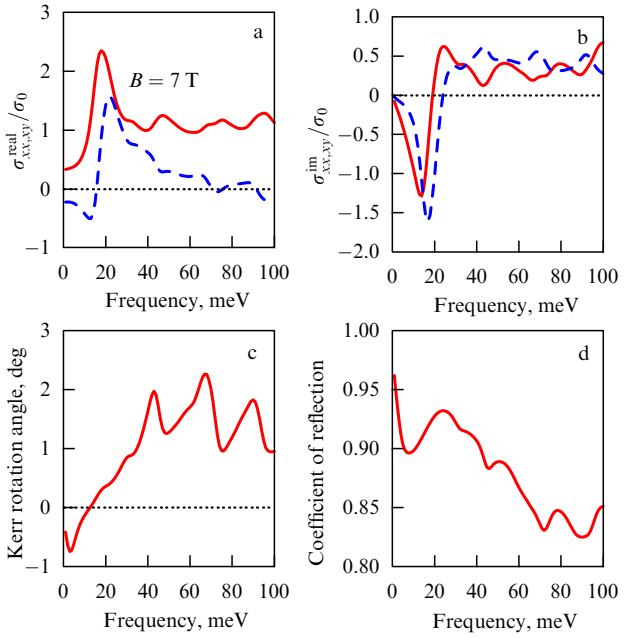

Figure 4. (a) Real and (b) imaginary parts of the longitudinal (xx), solid curve, and Hall (xy), dashed curve, dynamic conductivity of graphite. (c) Kerr rotation angle and (d) reflection coefficient in the magnetic field $B = 7$ T at the temperature $T = 0.1$ meV; the electronic relaxation frequency is $\Gamma = 3.5$ meV.

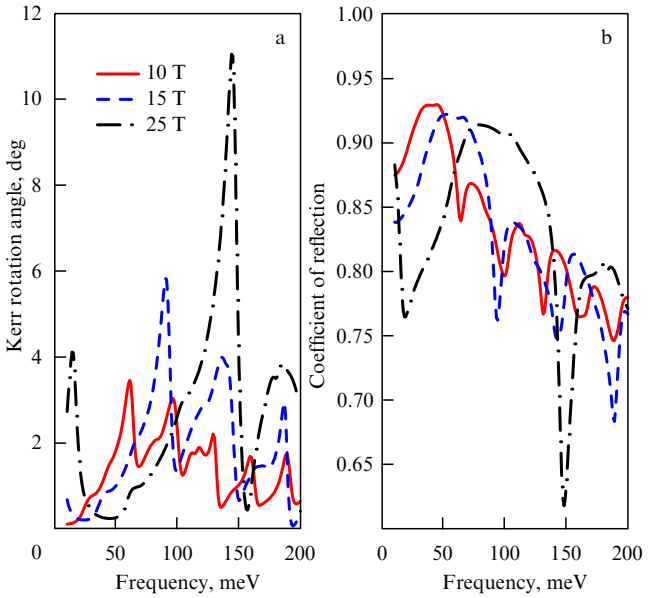

Figure 5. (a) Kerr rotation angle and (b) reflection coefficient of graphite in strong magnetic fields (10, 15, and 25 T) depending on the frequency of the electromagnetic wave.

table). The experimental values of the parameters γ_4, γ_5, and Δ exhibit a significant scatter; our values are close to those obtained in [17]. We note that in strong magnetic fields, the Fermi level increases to $\varepsilon_F \approx -1$ meV from the value given in the table for weak fields.

6. Conclusion

To the best of our knowledge, measurements of the Kerr and Faraday rotation angles in graphene layers have been made only at the University of Geneva, and we are grateful to A Kuzmenko and J Levallois for the fruitful discussions and for the opportunity to become acquainted with the experimental results before they were published.

Acknowledgments. This work was supported in part by the Russian Foundation for Basic Research (project No. 10-02-00193-a), by the National Research Foundation of Sweden (grant no. Scopes IZ73Z0_128026), and by the SIMTECH Program, New Century of Superconductivity: Ideas, Materials and Technologies (grant no. 246937).

References

1. Slonczewski J C, Weiss P R *Phys. Rev.* **109** 272 (1958)
2. Elias D C et al. *Nature Phys.* **7** 701 (2011)
3. Abrikosov A A, Beneslavskii S D *Zh. Eksp. Teor. Fiz.* **59** 1280 (1970) [*Sov. Phys. JETP* **32** 699 (1971)]
4. Mishchenko E G *Phys. Rev. Lett.* **98** 216801 (2007)
5. Falkovsky L A, Varlamov A A *Eur. Phys. J. B* **56** 281 (2007)
6. Gusynin V P, Sharapov S G, Carbotte J P *Phys. Rev. Lett.* **96** 256802 (2006)
7. Gusynin V P, Sharapov S G, Carbotte J P *Phys. Rev. B* **75** 165407 (2007)
8. Li Z Q et al. *Nature Phys.* **4** 532 (2008)
9. Falkovsky L A, Pershoguba S S *Phys. Rev. B* **76** 153410 (2007)
10. Kuzmenko A B et al. *Phys. Rev. Lett.* **100** 117401 (2008)
11. Nair R R et al. *Science* **320** 1308 (2008)
12. Mak K F et al. *Phys. Rev. Lett.* **101** 196405 (2008)
13. Falkovsky L A *Phys. Rev. B* **82** 073103 (2010)
14. Falkovsky L A *Zh. Eksp. Teor. Fiz.* **94** 783 (2011) [*JETP Lett.* **94** 723 (2011)]
15. Ozerin A Yu, Falkovsky L A, arXiv:1203.0157
16. Nakao K *J. Phys. Soc. Jpn.* **40** 761 (1976)
17. Doezema R E et al. *Phys. Rev. B* **19** 4224 (1979)
18. Mendez E, Misu A, Dresselhaus M S *Phys. Rev. B* **21** 827 (1980)
19. Kuzmenko A B et al. *Phys. Rev. B* **80** 165406 (2009)
20. Brandt N B, Chudinov S M, Ponomarev Ya G *Semimetals I. Graphite and its Compounds* (Amsterdam: Elsevier, 1988)
21. Crassee I et al. *Nature Phys.* **7** 48 (2011)

PACS numbers: 65.80.Ck, 72.15.Jf, 72.20.Pa, 72.80.Vp, 81.05.ue
DOI: 10.3367/UFNe.0182.201211j.1229

Anomalous thermoelectric and thermomagnetic properties of graphene

A A Varlamov, A V Kavokin,
I A Luk'yanchuk, S G Sharapov

1. Introduction

We present the results of recent investigations of some anomalies of thermoelectric and thermomagnetic properties of graphene. In Section 3, we show that the presence of a gap in the Dirac spectrum (the possibility of its existence under certain conditions is actively discussed in the literature) leads to the appearance of a characteristic peak in the thermopower as the chemical potential approaches the gap edge. The height of this peak can exceed the magnitude of the graphene thermopower, which is large by itself, by an order of magnitude. The giant effect revealed is related to the appearance, with the chemical potential approaching the edge of the gap, of a new channel of scattering of quasiparticles by impurities, with the relaxation time that essentially depends on energy. The analysis of this feature, which is based on the Kubo formalism, reproduces the well-known results for gapless graphene, but demonstrates the inapplicability of the simple Mott formula in the case under consideration.

In Section 4, we discuss the specific behavior of quantum oscillations of the Nernst coefficient (NC) that are observed in graphene and graphite upon the application of sufficiently strong magnetic fields. We show how the character of the spectrum of quasiparticles of a sample can be judged from the character of these oscillations.

2. On the history of thermoelectricity

The control of heat fluxes and the minimization of related losses are important factors in designing modern elements of nanoelectronics, including those based on the application of graphene [1]. Experiments [2] show that the thermoelectric effect can lead to a significant change in temperature (up to 30%) in the region of contacts and can therefore play a substantial role in the problem of cooling contacts. The experimentally measured magnitude of the graphene thermopower at room temperature can reach $k_B/e \sim 100$ μV K^{-1} (here, k_B is the Boltzmann constant and $-e < 0$ is the electron charge).

The study of thermoelectric and thermomagnetic phenomena has a two-century history. The thermoelectric effect, consisting in the appearance of electric current in a circuit that includes two different metals whose contacts are maintained at different temperatures, was discovered in 1821 by an Estonian–German scientist, Thomas Johann Seebeck. Quantitatively, the Seebeck effect is characterized by the differential thermopower (the Seebeck coefficient, i.e., the thermoelectromotive force arising in an inhomogeneously heated conductor) divided by the corresponding temperature difference:

$$S_{xx} = -\lim_{\Delta T \to 0} \frac{\Delta V}{\Delta T} = \frac{E_x}{\nabla_x T}\,.$$

The thermopower of metals is usually small (about 10^{-8} V K^{-1}), but can be much greater in doped semiconductors and in semimetals.

More than a century later [3], an English scientist, Nevill Mott, found an important relationship between the differential thermopower and the logarithmic derivative of the longitudinal electric conductivity $\sigma_{xx}(\mu, T)$ of a metal:

$$S_{xx}(\mu, T) = -\frac{\pi^2}{3e} k_B T \frac{\mathrm{d}}{\mathrm{d}\mu} \left[\ln \sigma_{xx}(\mu, T = 0)\right], \qquad (1)$$

where μ is the chemical potential of charge carriers and T is the temperature. At present, this formula is basic in analyzing experiments related to thermoelectricity; however, numerous anomalous situations are known where the behavior of the thermopower cannot be described by the Mott formula. These are phenomena such as an increase in the thermopower of metals at temperatures close to the Kondo temperature and the anomalies of thermopower at electron topological transitions and its oscillations in strong magnetic fields. One of the factors responsible for the invalidity of the Mott formula is the existence (due to one reason or another) of an essential dependence of the relaxation time of charge carriers on energy.

Among the variety of known thermomagnetic phenomena, those discussed most frequently are the effects of Nernst and Nernst–Ettingshausen, discovered by Austrian scientists Walter Nernst and Albert von Ettingshausen in 1886. The Nernst effect in metals [4], which is a thermal analog of the Hall effect, consists in the appearance of an electric field E_y perpendicular to the mutually perpendicular magnetic field H ($\|z$) and temperature gradient $\nabla_x T$. In this case, it is assumed that all electrical circuits are open, i.e., $J_x = J_y = 0$, and no heat flux is present along the y axis (the adiabaticity condition). Quantitatively, the effect is characterized by the NC

$$\nu = \frac{E_y}{(-\nabla_x T)\, H}\,.$$

Depending on the material, the NC can change within several orders of magnitude, from 7 μV K^{-1} T^{-1} in bismuth to 10^{-5} mB K^{-1} T^{-1} in "good" metals [5].

The Nernst–Ettingshausen effect is a different experimental realization of the Nernst effect: the electrical current is passed along the y axis through a sample placed into a magnetic field directed along the z axis; along the x axis, a

A A Varlamov National University of Science and Technology MISiS, Moscow, Russian Federation;
SPIN-CNR, University of Rome "Tor Vergata," Rome, Italy
E-mail: varlamov@ing.uniroma2.it
A V Kavokin University of Southhampton, UK;
St. Petersburg State University,
St. Petersburg, Russian Federation
I A Luk'yanchuk Landau Institute of Theoretical Physics, RAS, Moscow, Russian Federation;
University of Picardie Jules Verne, France
S G Sharapov Bogolyubov Institute for Theoretical Physics, National Academy of Sciences of Ukraine, Ukraine

Uspekhi Fizicheskikh Nauk **182** (11) 1229 – 1234 (2012)
DOI: 10.3367/UFNr.0182.201211j.1229
Translated by S N Gorin; edited A M Semikhatov

temperature gradient arises in this case. Below, we do not distinguish between these effects.

The microscopic nature of the Nernst effect remained unclear up to 1948, until Sondheimer [6], using a kinetic equation, found an expression for the NC of a degenerate electron gas with impurities by relating the NC to the derivative of the Hall angle $\theta_{\rm H} = \sigma_{xy}/\sigma_{xx}$ with respect to energy:

$$v(T) = -\frac{\pi^2}{3}\,\frac{cT}{eH_z}\,\frac{\partial}{\partial\mu}\left(\frac{\sigma_{xy}}{\sigma_{xx}}\right) = -\frac{\pi^2 T}{3m}\,\frac{{\rm d}\tau(\varepsilon)}{{\rm d}\varepsilon}\bigg|_{\varepsilon=\mu}, \qquad (2)$$

which permitted him to find the relation between these two effects and made the Nernst effect an important tool for studies of the character of scattering of charge carriers in semiconductors. In (2), m is the effective mass of charge carriers and $\tau(\varepsilon)$ is the energy-dependent relaxation time.

Within the Sondheimer theory, the coefficient v is constant in weak fields and decreases as H^{-2} in sufficiently strong fields, when the cyclotron frequency $\omega_{\rm c}$ exceeds τ^{-1} (the inverse relaxation time). In 1964, Obraztsov [7] noted the importance of taking so-called magnetization currents (electric currents arising because of the inhomogeneous magnetization of a sample) into account in discussing the Nernst effect.

In Sections 3 and 4, we present the results of two recent investigations [8, 9] of unusual thermoelectric and thermomagnetic effects in a ''hot'' field in the physics of condensed state, the study of properties of graphene and related systems.

3. Thermoelectric effect in graphene with a gap in its spectrum

The results of experiments [10–13] on the measurements of thermoelectric transport in graphene can mainly be explained theoretically using the Mott formula. Nevertheless, these experiments showed that Mott formula (1) gives results that do not correspond to experimental data when, at high temperatures, μ is close to the Dirac point, especially in graphene samples with a high mobility [13]. The theoretical analysis in [14–16] shows that this discrepancy is related to the violation of the conditions for the applicability of the Mott formula, which have the form $T \ll |\mu|$ and/or $T \ll \zeta$ (where ζ is the characteristic energy scale at which a change occurs in the conductivity $\sigma_{xx}(\mu, T = 0)$ near the Fermi surface).

Below, we show that the thermopower in graphene, which is already high, can be increased additionally by about an order of magnitude due to the opening of a gap Δ in the spectrum of quasiparticle excitations. This leads to the appearance of a new channel of scattering of quasiparticles, and because the relaxation time depends strongly on energy, this leads to the appearance of a giant peak in the thermopower when the chemical potential approaches the edge of the gap. This picture is very similar to the well-known thermopower anomaly near the electron topological transition (see review [17]).

We note that experiments [18, 19] indicate the presence of a gap in the spectrum of quasiparticle excitations in graphene near the Dirac point, which seems to be related to the effect of the substrate. For single-layer graphene, the problem of the existence of a gap has been studied insufficiently. Our results allow suggesting measurements of thermopower as a sensitive method for revealing the gap.

3.1 Electron scattering in gapped graphene

In the momentum representation, the Hamiltonian of graphene is written as

$$\widehat{H} = \sum_{\sigma}\int_{\rm BZ}\frac{{\rm d}^2 p}{(2\pi)^2}\,\Upsilon_\sigma^\dagger(\mathbf{p})\left[\widehat{\mathcal{H}}(\mathbf{p}) - \mu\,\widehat{\tau}_0\right]\Upsilon_\sigma(\mathbf{p}), \qquad (3)$$

where

$$\widehat{\mathcal{H}}(\mathbf{p}) = \widehat{\tau}_+\phi(\mathbf{p}) + \widehat{\tau}_-\phi^*(\mathbf{p}) + \Delta\,\widehat{\tau}_3,$$

$\widehat{\tau}_0$, $\widehat{\tau}_3$, and $\widehat{\tau}_\pm = (\widehat{\tau}_1 \pm {\rm i}\,\widehat{\tau}_2)/2$ are the Pauli matrices acting in the space of sublattices on the spinors $\Upsilon_\sigma(\mathbf{p})$ and $\Upsilon_\sigma^\dagger(\mathbf{p}) = \left(a_\sigma^\dagger(\mathbf{p}),\, b_\sigma^\dagger(\mathbf{p})\right)$ with the electron creation (annihilation) operators $a_\sigma^\dagger(\mathbf{p})$ and $b_\sigma^\dagger(\mathbf{p})$ $\left(a_\sigma(\mathbf{p})\right.$ and $\left.b_\sigma(\mathbf{p})\right)$, which correspond to the sublattices of components A and B; σ is the spin index; and the integration is performed over the Brillouin zone (BZ). In the case under consideration, the complex function $\phi(\mathbf{p})$ responsible for the dispersion can be chosen near two independent K points of the BZ in the form $\xi \equiv |\phi(\mathbf{p})| = \hbar v_{\rm F}|\mathbf{p}|$, where $v_{\rm F}$ is the Fermi velocity, and the wave vector $\mathbf{p}$ is referenced to the corresponding K point. The presence of the gap Δ violates the equivalence of the A and B sublattices, and the spectrum near the K points takes the form $E(\mathbf{p}) = \pm(\hbar^2 v_{\rm F}^2\mathbf{p}^2 + \Delta^2)^{1/2} - \mu$.

Scattering by impurities is considered using the Abrikosov–Gor'kov technique in terms of the self-consistent Born approximation. The scattering potential is chosen such that the scattering between different valleys can be neglected; within a single valley, the potential is assumed to be constant, equal to $u(\mathbf{0})$. As a result, we obtain the following expression for the scattering by impurities:

$$\Gamma(\varepsilon) = \Gamma_0\left(\frac{|\varepsilon+\mu|}{|\mu|} + \frac{\Delta^2}{|\varepsilon+\mu||\mu|}\right)\theta\left((\varepsilon+\mu)^2 - \Delta^2\right), \qquad (4)$$

where $\Gamma_0 = 2\hbar/\tau_0$, τ_0 is the characteristic relaxation time, $\tau_0^{-1} = n_i|u(\mathbf{0})|^2|\mu|/(4\hbar^3 v_{\rm F}^2)$ [20], n_i is the concentration of charge carriers, and θ is the Heaviside function. In the results presented below, we use the value $\Gamma_0 = 20$ K, neglecting the concentration dependence. It follows from Eqn (4) that the scattering is absent at $(\varepsilon+\mu)^2 < \Delta^2$. Nevertheless, we note that some processes that have not been taken into account in the model lead to a finite relaxation time below the edge of the gap. In numerical calculations, this is taken into account by adding a small residual scattering γ_0 to $\Gamma(\varepsilon)$. The final results are almost independent of γ_0.

3.2 Thermopower in gapped graphene

Using the Kubo formula, the following expressions can be obtained for the electrical conductivity and thermoelectric coefficient:

$$\left\{\begin{matrix}\sigma_{xx}\\ \beta_{xx}\end{matrix}\right\} = \frac{e^2}{\hbar}\int_{-\infty}^{\infty}\frac{{\rm d}\varepsilon\,\mathcal{A}\left(\varepsilon,\Gamma(\varepsilon),\Delta\right)}{2T\cosh^2\left[\varepsilon/(2T)\right]}\left\{\begin{matrix}1\\ \varepsilon\\ \overline{eT}\end{matrix}\right\}, \qquad (5)$$

where at a nonzero gap Δ, the function $\mathcal{A}$ has the form [21, 22]

$$\mathcal{A}(\varepsilon,\Gamma(\varepsilon),\Delta) = \frac{1}{2\pi^2}\left[1 + \frac{(\mu+\varepsilon)^2 - \Delta^2 + \Gamma^2(\varepsilon)}{2|\mu+\varepsilon|\,\Gamma(\varepsilon)} \times\left(\frac{\pi}{2} - \arctan\frac{\Delta^2 + \Gamma^2(\varepsilon) - (\mu+\varepsilon)^2}{2|\mu+\varepsilon|\,\Gamma(\varepsilon)}\right)\right]. \qquad (6)$$

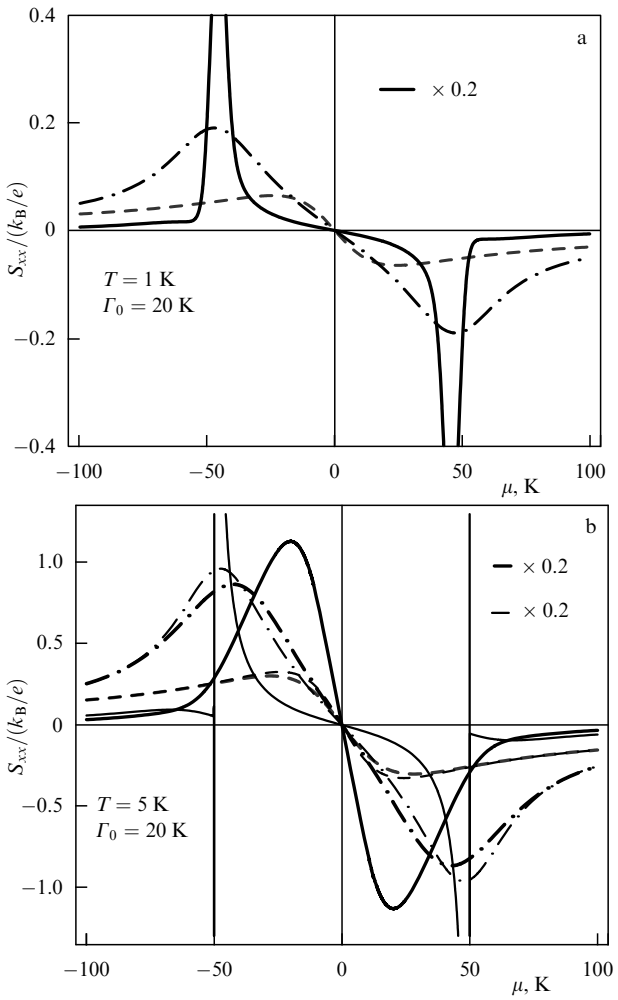

Figure 1. (Available in color online.) Thermopower S_{xx} (in k_B/e units) as a function of the chemical potential μ at (a) $T = 1$ K and (b) $T = 5$ K. The dashed curves correspond to the energy-independent $\Gamma = \Gamma_0$ and $\Delta = 0$; dashed-dotted thick curves to $\Gamma = \Gamma_0$ and $\Delta = 50$ K; solid thick curves to the energy-dependent $\Gamma(\varepsilon)$ and $\Delta = 50$ K. The dependences shown by continuous lines are multiplied by 0.2. The thin curves in (b) are obtained via the Mott formula.

At $\Delta = 0$, Eqn (6) is simplified to the form considered in [14, 16]. In this case, assuming that $\Gamma(\varepsilon) = \Gamma_0 = \text{const}$ and that $|\mu| \gg T$, Γ_0, we find that $\sigma_{xx} = e^2|\mu|/(2\pi\hbar\Gamma_0)$ and $\beta_{xx} = \pi e T \operatorname{sgn}\mu/(6\hbar\Gamma_0)$, in accordance with the results in [22]. Then the thermopower $S_{xx} = -\beta_{xx}/\sigma_{xx}$ is the same as in usual metals, $S_{xx} = -(\pi^2/3e)\,T/\mu$, and coincides with the value that directly follows from Mott formula (1).

The $S_{xx}(\mu)$ dependences at $T = 1$ K and $T = 5$ K are shown in Fig. 1. The thick dashed curves correspond to the case $\Delta = 0$, $\Gamma(\varepsilon) = \Gamma_0$, with $\sigma_{xx}(\mu) \propto |\mu|$ and $S_{xx}(\mu) \propto 1/\mu$ at large $|\mu|$. Expressions (5) and (6) also allow reproducing the results in the case of a nonzero gap and an energy-independent $\Gamma(\varepsilon) = \Gamma_0$ [21, 22]. The corresponding dependences are shown by thick dashed-dotted curves, calculated at $\Delta = 50$ K.

Our main result, shown by thick solid curves, was obtained for the energy-dependent $\Gamma(\varepsilon)$ given by Eqn (4), at $\Delta = 50$ K. We note that the corresponding values of $S_{xx}(\mu)$ were diminished fivefold to show them together with the other curves in the figure. This means that the peak values of the thermopower are at least fivefold greater than the magnitude of the thermopower obtained for $\Gamma(\varepsilon) = \text{const}$.

A substantial increase in the thermopower in the case of the energy-dependent $\Gamma(\varepsilon)$ can already be expected on the basis of Mott formula (1). Nevertheless, formula (1) cannot be used for a quantitative description. Indeed, the thin curves in Fig. 1b were obtained with the use of data for the electrical conductivity at the zero temperature $\sigma(\mu, T = 0) = (2e^2/\hbar)\,\mathcal{A}(0, \Gamma(0), \Delta)$ and Mott formula (1), whereas the thick curves were derived using the Kubo formula for both σ_{xx} and β_{xx}. It is seen that the agreement between the Kubo and Mott formulas is quite good for $\Delta = 0$ and $\Gamma(\varepsilon) = \text{const}$, and becomes ideal at $T = 1$ K; therefore, the results for the Mott formula are not given in Fig. 1a. At the same time, it can be seen from Fig. 1b that for a finite value of Δ and $\Gamma(\varepsilon) = \text{const}$, a discrepancy is already observed between the results obtained using the Kubo and Mott formulas, especially near $|\mu| = \Delta$. Finally, in the case of an energy-dependent $\Gamma(\varepsilon)$, the Mott formula is inapplicable.

A specific feature of thermopower is its sensitivity to the derivative of the reciprocal relaxation time. Therefore, the presence of the θ function in (4) strongly affects the $S(\mu)$ dependence near $|\mu| \approx \Delta$. Here, it is worth mentioning once again that an obvious analogy exists between the transport in gapped graphene and in metals near the topological electron transition. Indeed, near the critical value of the chemical potential $\mu = \mu_c$, where the connectivity of the Fermi surface changes, the relaxation time of quasiparticles becomes substantially energy-dependent, which leads to the appearance of well-known bends in the conductivity curves and of peaks in the thermopower [17].

4. Giant oscillations of the NC in graphene

Giant oscillations of the NC were discovered in 1959 in [25], where this phenomenon was explained as the intersection of the chemical potential by the Landau levels. As in the case of the de Haas–van Alphen oscillations of magnetization and the Shubnikov–de Haas oscillations of conductivity, the fields corresponding to the oscillations of the NC are determined by the Lifshits–Onsager condition [23]

$$S(\mu) = (k + \gamma_\sigma)\, 2\pi\hbar\, \frac{eH_{k\sigma}}{c}\,, \tag{7}$$

where $S(\mu)$ is the area of the Fermi surface cross section corresponding to the orbital motion of electrons at $p_z = 0$, k is an integer, $\gamma_\sigma = \gamma + 1/2\,(m^*/m)\,\sigma$ with $\sigma = \pm 1$, and $m^* = (1/2\pi)\,\mathrm{d}S/\mathrm{d}\mu$ is the cyclotron mass of the electron [23].

Quite recently, the Nernst effect in graphene was studied experimentally [11, 12] and the corresponding results were analyzed in terms of the standard theory [24]. Unexpectedly, it was found that under oscillations, the NC changes sign in graphene in fields that satisfy condition (7), whereas in zinc [25] and bismuth [26], maxima are observed in the corresponding fields. This unusual behavior of the $\nu(H)$ oscillations in graphene is not reproduced in three-dimensional graphite.

One more remarkable property of quantum oscillations is the dependence of their character on the type of the spectrum of charge carriers, namely, on the value of the topological parameter γ [27, 28]: $\gamma = 1/2$ for normal charge carriers (NCCs) with a parabolic two-dimensional (2D) spectrum and Landau linear quantization:

$$\text{NC}: \quad \varepsilon(p_\perp) = \frac{p_\perp^2}{2m_\perp}\,, \quad \varepsilon_k = 2\mu_B\, H\, \frac{m}{m_\perp}\left(k + \frac{1}{2}\right),$$

and $\gamma = 0$ for Dirac fermions (DFs), which have a linear spectrum with two branches and a square-root dependence of the energy of Landau levels ($\sim k^{1/2}$) in a magnetic field:

$$\text{DF}: \quad \varepsilon(p_\perp) = \pm v|p_\perp|\,, \quad \varepsilon_k = \pm\left(4mv_\text{F}^2\,\mu_\text{B}\,Hk\right)^{1/2},$$

where $p_\perp$ and $m_\perp$ are the momentum and the effective mass in the plane perpendicular to the magnetic field, m is the mass of a free electron, v_F is its Fermi velocity, and $\mu_\text{B} = e/2mc$ is the Bohr magneton.

Below, we use a simple thermodynamic approach to the description of the Nernst effect, which allows relating the corresponding oscillations to the de Haas–van Alphen oscillations of magnetization. For both contributions to the NC — the thermal contribution (Sondheimer [6]) and the contribution corresponding to magnetization currents (Obraztsov [7]) — exact expressions are found for both parabolic and Dirac spectra. In the last case, our results quite well reproduce the oscillations of the NC found experimentally in graphene [11, 12]. It is remarkable that in contrast to the case of a parabolic spectrum, their amplitude decreases rather than increases with increasing the Fermi energy (gate voltage). The shape of the oscillations is determined by the temperature derivative of the de Haas–van Alphen oscillations.

4.1 Thermodynamic description of the Nernst effect

As mentioned in Section 2, the NC is measured in the absence of currents in the system. Therefore, the electrochemical potential along the temperature gradient can be considered constant, $\mu + e\varphi = \text{const}$ (where φ is the electrostatic potential). Consequently, the effect of temperature inhomogeneity in the sample is determined by the appearance of an effective electric field $E_x = \nabla_x \mu/e$ along the temperature gradient. The problem therefore reduces to the classical Hall problem, which allows easily finding the thermal contribution to the NC,

$$v^\text{term} = \frac{\sigma_{xx}}{e^2 nc}\,\frac{\mathrm{d}\mu}{\mathrm{d}T}\,, \tag{8}$$

where n is the concentration of charge carriers. This simple formula reproduces the Sondheimer result for a degenerate electron gas, the fluctuation contribution to the NC in superconductors at temperatures above T_c, etc. [30].

The second contribution to the NC, which arises as a result of the spatial dependence of magnetization in the sample [7], can be found based on the Ampère law. The density of the magnetization current is written as $\mathbf{j}^\text{mag} = [c/(4\pi)]\,\nabla \times \mathbf{B}$, where $\mathbf{B} = \mathbf{H} + 4\pi\mathbf{M}$, $\mathbf{H}$ is the spatially homogeneous magnetic field, and $\mathbf{M}$ is the magnetization, which can depend on temperature and hence on the coordinates. The magnetization-related current density is written as $j_y^\text{mag} = -c(\mathrm{d}M/\mathrm{d}T)\,\nabla_x T$; the corresponding contribution to the Nernst electric field is $E_y^\text{mag} = \rho_{yy} j_y^\text{mag}$, where ρ_{yy} is the diagonal component of the resistivity ($\rho_{yy} = \rho_{xx}$). As a result, the contribution from the magnetization currents to the NC is written as

$$v^\text{mag} = \frac{c\rho_{yy}}{H}\left(\frac{\mathrm{d}M}{\mathrm{d}T}\right). \tag{9}$$

Relations (8) and (9) allow elucidating the physical nature of oscillations of the NC in quantizing magnetic fields. In particular, they show that the NC depends on the diagonal components of the conductivity and resistivity tensors, whose oscillations, depending on the magnetic field, are nothing more than the Shubnikov–de Haas effect. However, in graphene, the giant oscillations of the NC are also observed in the state where the Shubnikov–de Has effect is small (at $H < 3$ T) [12]; we should therefore assume that the giant oscillations of the NC in the last case are due to other factors in expressions (8) and (9), namely, the temperature derivatives of the chemical potential $\mathrm{d}\mu/\mathrm{d}T$ and magnetization $\mathrm{d}M/\mathrm{d}T$. It is remarkable that to obtain explicit expressions for these quantities, we need no additional information on the transport properties of the system; these derivatives can be expressed in terms of the thermodynamic potential Ω:

$$\frac{\mathrm{d}\mu}{\mathrm{d}T} = \frac{\partial^2\Omega}{\partial T\,\partial\mu}\left(\frac{\partial^2\Omega}{\partial\mu^2}\right)_T^{-1}, \qquad \frac{\mathrm{d}M}{\mathrm{d}T} = \frac{\partial^2\Omega}{\partial T\,\partial H}\,. \tag{10}$$

The expression for the oscillating part of the thermodynamic potential in the case of a parabolic spectrum obtained in [31] (see also [32]) was later extended to an arbitrary spectrum $\varepsilon_\perp(p_\perp)$ in [33] (see also [34]). In the 2D case, we have

$$\widetilde{\Omega} = \frac{m^*}{2\pi\hbar^2}\,\frac{\hbar^2\omega_\text{c}^2}{\pi^2}\,\frac{1}{2}\sum_{l=1,\,\sigma=\pm1}^{\infty}\frac{\psi(\lambda l)}{l^2}\exp\left(-\frac{2\pi l\Gamma}{\hbar\omega_\text{c}}\right) \times\cos\left[2\pi l\left(\frac{c}{e\hbar}\,\frac{S(\mu)}{2\pi H}-\gamma_\sigma\right)\right], \tag{11}$$

with $\psi(\lambda l) = \lambda l/\sinh\lambda l$. Here, $\lambda = 2\pi^2 T/(\hbar\omega_\text{c})$ and Γ is the Dingle broadening of the Landau level. To apply the results to both the parabolic and Dirac spectra, we represent expression (11) in the most general form using the parameters S, m^*, ω_c, and γ_σ. In the case of NCCs, we have $S = 2\pi m_\perp\,\mu$, $m^* = m_\perp$, $\omega_\text{c} = eH/m_{\perp\text{c}}$, and $\gamma_\sigma = 1/2 + (1/2)\,(m_\perp/m)\,\sigma$; in the case of DFs, $S = \pi\mu^2/v^2$, $m^* = \mu/v^2$, $\omega_\text{c} = eHv^2/(\mu c)$, and $\gamma_\sigma = 1/2\,[\mu/(mv^2)]\,\sigma$. As a result, the oscillating parts of the magnetization and chemical potential can be expressed, using relation (10), in the form

$$\frac{\mathrm{d}\widetilde{\mu}}{\mathrm{d}T} = -\frac{\operatorname{Im}\Xi^{\{1\}}}{1+2\operatorname{Re}\Xi^{\{0\}}}\,, \quad \frac{\mathrm{d}\widetilde{M}}{\mathrm{d}T} = \frac{n}{H}\,\frac{\mathrm{d}\widetilde{\mu}}{\mathrm{d}T}\,, \tag{12}$$

where

$$\Xi^{\{\alpha\}} = \frac{1}{2}\sum_{l=1,\,\sigma=\pm1}^{\infty}\psi^{(\alpha)}(\lambda l)\exp\left(-\frac{2\pi l\Gamma}{\hbar\omega_\text{c}}\right) \times\cos\left[2\pi l\left(\frac{c}{e\hbar}\,\frac{S(\mu)}{2\pi H}-\gamma_\sigma\right)\right], \tag{13}$$

and $\psi^{(\alpha)}(x)$ is the derivative of ψ of the order $\alpha = 0, 1$. It follows from (9) and (12) that the NC oscillates proportionally to the temperature derivative of the magnetization. This fact suggests the existence of an important universal (independent of the dimensionality and type of charge carriers) relation between the oscillations of the NC and the de Haas–van Alphen effect.

It is convenient to represent the NC in the form

$$v = v^\text{term} + v^\text{mag} = v_0(H) + \widetilde{v}(H)\,, \tag{14}$$

where $v_0(H)$ and $\widetilde{v}(H)$ are respectively the background and oscillating parts. The background part can be found in the Drude theory approximation [30]:

$$v_0(H) = \frac{\pi^2\tau}{6m^*c}\left(\frac{T}{\varepsilon_\text{F}}\right)\frac{1}{1+(\omega_\text{c}\tau)^2}\,. \tag{15}$$

Taking the magnetization currents into account here leads to the appearance of a correction to Sondheimer's result (15) of the order $(\varepsilon_F\tau)^{-2}$.

With (8), (9), and (12), the oscillating part of the NC can be represented as

$$\tilde{\nu}(H) = -2\pi\kappa(H)\frac{\operatorname{Im}\Xi^{\{1\}}}{1+2\operatorname{Re}\Xi^{\{0\}}}, \qquad (16)$$

where

$$\kappa(H) = \frac{\sigma_{xx}(H)}{e^2nc} + \frac{cn\rho_{xx}(H)}{H^2}. \qquad (17)$$

Expression (16) describes the oscillations of the NC in the most general form, which is valid for an arbitrary type of the spectrum of charge carriers $\varepsilon_\perp(p_\perp)$.

4.2 Shape of oscillations and its dependence on the type of carriers

We analyze expression (16) in the limit of low temperatures, $2\pi^2T < \hbar\omega_c$. In this case, the parameter λ in (11) is much less than unity; consequently, $\psi(\lambda l) \approx 1 - (1/6)\lambda^2l^2$. For $m^* < 0.02m$ and $H = 10$ T (typical values in experiments on graphene), this requirement means that $T < 10$ K. Because $m^* \ll m$, we can neglect the Zeeman splitting, assuming that $\gamma_\sigma = 0$ for the NCCs and $\gamma_\sigma = 1/2$ for the DFs. The series $\Xi^{\{0\}}$ and $\Xi^{\{1\}}$ in (16) in this case can be summed analytically:

$$\tilde{\nu}^{(2D)}(\mu, H) = \frac{2\pi^3}{3}\frac{T}{\hbar\omega_c}\kappa(H) \times \frac{\sin 2\pi\{[c/(e\hbar)]\,[S(\mu)/(2\pi H)] - \gamma\}}{\cosh[2\pi\Gamma/(\hbar\omega_c)] - \cos 2\pi\{[c/(e\hbar)][S(\mu)/(2\pi H)] - \gamma\}}. \qquad (18)$$

In experiments involving measurements of the NC in graphene, the number of particles is usually fixed; therefore, we have the relation [31]

$$n = -\left(\frac{\partial\Omega(\mu)}{\partial\mu}\right)_{H,T} = 2\frac{S(\mu)}{(2\pi\hbar)^2} - \left(\frac{\partial\tilde{\Omega}(\mu)}{\partial\mu}\right)_{H,T} = \text{const} \qquad (19)$$

(we assume that the volume is $V = 1$). This equation implicitly determines the dependence of the chemical potential μ on H and T at a given n. We note that according to (19), the chemical potential μ is a function of the magnetic field H. The corresponding expression for $S(\mu)$ is

$$\frac{c}{e\hbar}\frac{S(\mu)}{2H} = \pi^2\frac{\hbar c}{e}\frac{n}{H} - \arctan\frac{\sin 2\pi[\pi(\hbar c/e)\,n/H - \gamma]}{\exp(2\pi\Gamma/\hbar\omega_c) + \cos 2\pi[\pi(\hbar c/e)\,n/H - \gamma]}. \qquad (20)$$

Relation (20) gives the sought dependence $\mu(n, H)$. Substituting (20) in (18), after laborious calculations, we can find the oscillating part of the NC in the explicit form

$$\tilde{\nu}^{(2D)}(n, H) = \frac{2\pi^3}{3}\frac{T}{\hbar\omega_c}\frac{\kappa(H)}{\sinh(2\pi\Gamma/\hbar\omega_c)} \times \sin 2\pi\left(\pi\frac{\hbar c}{e}\frac{n}{H} - \gamma\right). \qquad (21)$$

We see that Eqn (21) is a strongly oscillating function that vanishes in magnetic fields in which Landau levels cross the chemical potential ($H = H_{k\sigma}$ is determined by condition (7)). The magnetic-field-dependent factor $\kappa(H)$, which is determined by the behavior of magnetoresistance, is given by (17). At $\omega_c\tau \leqslant 1$, when the Shubnikov–de Haas oscillations are small, $\kappa(H)$ can be estimated in the Drude approximation. In particular, in the limit where $\omega_c\tau \sim 1$, we obtain $\kappa(H) \sim \tau/(m^*c)$ (assuming that $\Gamma \sim \hbar/2\tau$), and the amplitude of NC oscillations turns out to be giant compared to the background magnitude $\tilde{\nu}^{(2D)} \sim [\varepsilon_F/(\hbar\omega_c)]\,\nu_0$. In stronger fields ($\omega_c\tau > 1$), under the quantum Hall effect, the shape of NC oscillations begins to be determined by the sharp dependence of the magnetoconductivity and of the Dingle temperature on the magnetic field. This circumstance can be taken into account by substituting the appropriate dependences in Eqns (16) and (17).

Figure 2a displays the oscillations of the NC as a function of the inverse magnetic field for the two-dimensional system with parabolic and Dirac spectra in accordance with Eqn (21). Both theoretical and experimental results obtained for graphene [11, 12] exhibit a sinusoidal profile of the signal,

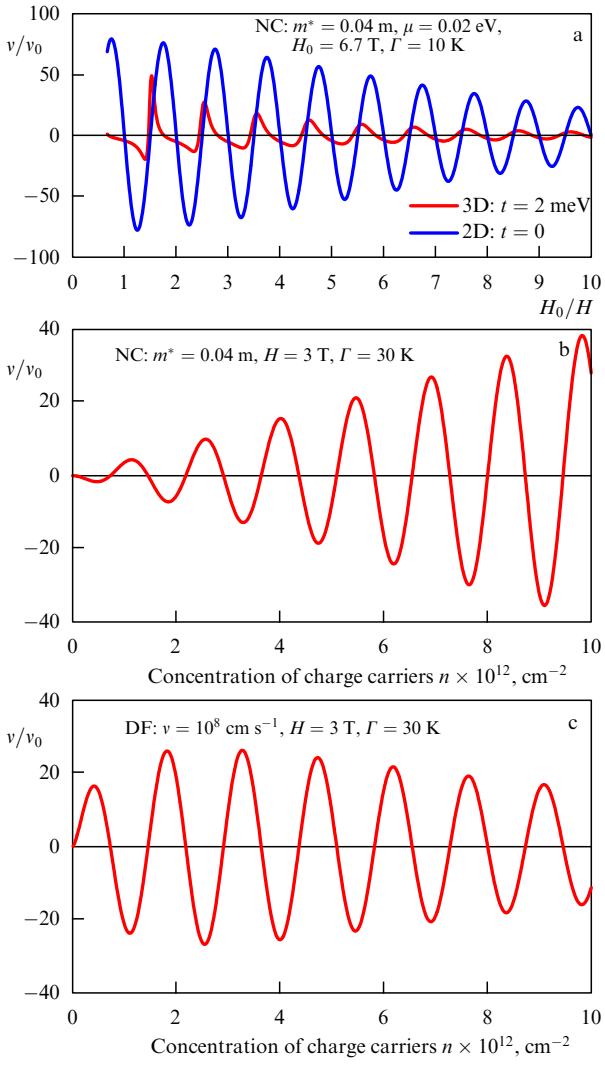

Figure 2. (a) Oscillations of the NC as a function of the inverse magnetic field and the concentrations of charge carriers (b) with a parabolic spectrum (NCC) and (c) for Dirac fermions (DF). The $\nu(H^{-1})$ dependence for the DFs has the same shape as the dependence for the NCCs, but is shifted relative to the latter by a half-period. The vertical straight lines indicate the field values at which quantization condition (7) is satisfied.

whose amplitude decreases slowly with increasing the concentration of charge carriers with the Dirac spectrum. This behavior contradicts the theoretical predictions based on the classical Mott formula applied to the Boltzmann electron gas [11]. On the contrary, in the case of charge carriers with a parabolic spectrum, our theory predicts an increase in the amplitude of oscillations with increasing the concentration of charge carriers. The last statement agrees qualitatively with the results obtained using the Mott formula.

Acknowledgments. This work was supported in part by the SIMTECH project (New Century of Superconductivity: Ideas, Materials and Technologies) No. 246937 within the European program FP7.

References

1. Geim K L *Science* **324** 1530 (2009)
2. Grosse K L et al. *Nature Nanotechnol.* **6** 287 (2011)
3. Mott N F, Jones H *The Theory of the Properties of Metals and Alloys* 1st ed. (Oxford: Clarendon Press, 1936)
4. Von Ettingshausen A, Nernst W *Ann. Physik* **265** 343 (1886)
5. Behnia K, Méasson M-A, Kopelevich Y *Phys. Rev. Lett.* **98** 076603 (2007)
6. Sondheimer E H *Proc. R. Soc. London A* **193** 484 (1948)
7. Obraztsov Yu N *Fiz. Tverd. Tela* **6** 414 (1964) [*Sov. Phys. Solid State* **6** 331 (1964)]
8. Sharapov S G, Varlamov A A *Phys. Rev. B* **86** 035430 (2012)
9. Luk'yanchuk I A, Varlamov A A, Kavokin A V *Phys. Rev. Lett.* **107** 016601 (2011)
10. Wei P et al. *Phys. Rev. Lett.* **102** 166808 (2009)
11. Zuev Y M, Chang W, Kim P *Phys. Rev. Lett.* **102** 096807 (2009)
12. Checkelsky J G, Ong N P *Phys. Rev. B* **80** 081413(R) (2009)
13. Wang D, Shi J *Phys. Rev. B* **83** 113403 (2011)
14. Löfwander T, Fogelström M *Phys. Rev. B* **76** 193401 (2007)
15. Hwang E H, Rossi E, Das Sarma S *Phys. Rev. B* **80** 235415 (2009)
16. Ugarte V, Aji V, Varma C M *Phys. Rev. B* **84** 165429 (2011)
17. Varlamov A A, Egorov V S, Pantsulaya A V *Adv. Phys.* **38** 469 (1989)
18. Zhou S Y et al. *Nature Mater.* **6** 770 (2007)
19. Li G, Luican A, Andrei E Y *Phys. Rev. Lett.* **102** 176804 (2009)
20. Peres N M R, Lopes dos Santos J M B, Stauber T *Phys. Rev. B* **76** 073412 (2007)
21. Gorbar E V et al. *Phys. Rev. B* **66** 045108 (2002)
22. Gusynin V P, Sharapov S G *Phys. Rev. B* **71** 125124 (2005); *Phys. Rev. B* **73** 245411 (2006)
23. Lifshits I M, Kosevich A M *Zh. Eksp. Teor. Fiz.* **29** 730 (1955) [*Sov. Phys. JETP* **2** 636 (1956)]
24. Bergman D L, Oganesyan V *Phys. Rev. Lett.* **104** 066601 (2010)
25. Bergeron C J, Grenier C G, Reynolds J M *Phys. Rev. Lett.* **2** 40 (1959)
26. Behnia K, Méasson M-A, Kopelevich Y *Phys. Rev. Lett.* **98** 166602 (2007)
27. Falkovsky L A *Zh. Eksp. Teor. Fiz.* **49** 609 (1965) [*Sov. Phys. JETP* **22** 423 (1966)]
28. Mikitik G P, Sharlai Yu V *Phys. Rev. Lett.* **82** 2147 (1999)
29. Serbyn M N et al. *Phys. Rev. Lett.* **102** 067001 (2009)
30. Varlamov A A, Kavokin A V *Europhys. Lett.* **86** 47007 (2009)
31. Champel T, Mineev V P *Phylos. Mag. B* **81** 55 (2001)
32. Bratkovsky A M, Alexandrov A S *Phys. Rev. B* **65** 035418 (2002)
33. Luk'yanchuk I A, Kopelevich Y *Phys. Rev. Lett.* **93** 166402 (2004)
34. Sharapov S G, Gusynin V P, Beck H *Phys. Rev. B* **69** 075104 (2004)